Journal of Materials Chemistry B

PAPER

View Article Online
View Journal | View Issue

Cite this: J. Mater. Chem. B, 2014, 2, 739

Preparation of core–shell Fe_3O_4@poly(dopamine) magnetic nanoparticles for biosensor construction†

Miriam Martín,[ab] Pedro Salazar,*[ac] Reynaldo Villalonga,[d] Susana Campuzano,[d] José Manuel Pingarrón[d] and José Luis González-Mora[a]

Received 21st August 2013
Accepted 21st November 2013

DOI: 10.1039/c3tb21171a

www.rsc.org/MaterialsB

Novel core–shell Fe_3O_4@poly(dopamine) magnetic nanoparticles were prepared through an *in situ* self-polymerization method. The hybrid nanomaterial showed an average core diameter of 11 ± 3 nm and a polymer thin film thickness of 1.8 ± 0.2 nm. The core–shell nanoparticles were employed as solid supports for the covalent immobilization of horseradish peroxidase (HRP), and the resulting biofunctionalized magnetic nanoparticles were employed to construct an amperometric biosensor for H_2O_2. The enzyme biosensor showed a high sensitivity of 442.14 mA M^{-1} cm^{-2}, a low limit of detection of 182 nM, a wide linear range from 6.0×10^{-7} to 8.0×10^{-4} M and high stability for 1 month.

Introduction

During recent decades, iron oxide-based magnetic nanoparticles have attracted much attention in biomedical, analytical, environmental and industrial applications due to their easy and controlled synthesis and surface modification, high biocompatibility and low toxicity.[1–4] Moreover, their magnetic properties add a new dimension for biomedical and analytical applications such as in immunoprecipitation and separation techniques, drug delivery, magnetic resonance imaging and hyperthermia treatments.[5–10]

Magnetic nanoparticles have been widely employed in electrochemical biosensors as nanosized supports for the immobilization of analytical biomolecules.[11–14] In particular, the immobilization of enzymes on the surface of these nanoparticles offers numerous advantages including enhancement of the enzymatic activity and reduction of the mass-transfer processes associated with the recognition of substrates by enzymes. Iron oxide nanoparticles also provide a favorable microenvironment for electrochemical devices where enzymes may exchange electrons directly with the transducer, improving the sensitivity and selectivity of electrochemical biosensors.[15–17] In this way, a great number of electrochemical biosensors using modified Fe_3O_4 nanoparticles have been reported in the literature for sulfite, phenolic compounds, glucose, lactate, H_2O_2, *etc.*[17–21]

Enzyme-modified magnetic nanoparticles can be prepared by adsorption of proteins on the nanoparticle surface through the combined contribution of electrostatic interactions, hydrogen bonding, van-der-Waals forces and hydrophobic interactions. However, these interactions can be affected by pH, ionic strength, temperature and polarity of solvents. Consequently, such an immobilization procedure often yields less stable catalysts due to the lack of enzyme molecules on the support.[22] Stable enzyme–magnetic nanoparticle adducts can be prepared by covalent immobilization approaches. In general, these procedures require several reaction steps for nanoparticle surface modification and enzyme immobilization, increasing the complexity of the enzyme-modified nanoparticle synthesis and thus affecting the catalytic activity of the final adduct.[22] For these reasons, the development of novel methods for the covalent functionalization of magnetic nanoparticles with enzymes receives considerable attention.

Dopamine (DA) is a catecholamine neurotransmitter related to many physiological processes and neurophysiological disorders such as schizophrenia, Parkinson's and Alzheimer's diseases, as well as several social and addiction behaviors.[23–25] In addition to its biomedical relevance, DA has been recently proposed as a novel organic coating material. Messersmith's group reported that DA can be self-polymerized in aerated basic solutions, forming an adherent poly(dopamine) (pDA) film over a wide variety of organic and inorganic surfaces.[26,27] Although the structure of this polymeric film has not been yet elucidated, it is probably formed by reaction of the primary amino groups and quinone groups of oxidized DA *via* the formation of Schiff bases and/or Michaelis addition adducts.[26,27]

[a]*Neurochemistry and Neuroimaging group, Faculty of Medicine, University of La Laguna, Tenerife, Spain. E-mail: psalazar@ull.edu.es*

[b]*Atlántica Biomédica, Tenerife, Spain*

[c]*Informática y Equipamiento Médico de Canarias, Tenerife, Spain*

[d]*Department of Analytical Chemistry, Faculty of Chemistry, Complutense University of Madrid, 28040, Madrid, Spain*

† Electronic supplementary information (ESI) available. See DOI: 10.1039/c3tb21171a

The reactive quinones at the surface of pDA films could be used as anchoring points for further chemical modification and/or immobilization of biologically active macromolecules (antibodies, enzymes, *etc.*).[28–30] Poly(dopamine)-mediated surface modification has been demonstrated to provide versatile platforms for DNA immobilization,[31] efficient and reliable manipulation of human neural stem cells (NSCs),[32] growth factor immobilization, hematopoietic cell adhesion, antibacterial surface preparations[33] and hydroxyapatite crystallization.[34] Other approaches, using non-polymerized DA or L-dopa, have been demonstrated to be useful for the functionalization of magnetic nanoparticles, allowing their use as solid supports for enzyme immobilization.[35,36] However these protocols are laborious and lengthy (4–5 working days)[35] and require glutaraldehyde as a coupling agent.[36]

In this work we describe the preparation and characterization of core–shell Fe_3O_4@pDA magnetic nanoparticles and their use in the construction of an electrochemical enzyme biosensor. In contrast to other reported protocols,[35,36] the methodology described in this work is rapid (3 h) and direct, not requiring further surface activation or treatment with additional coupling agents. As a proof-of-concept, horseradish peroxidase (HRP) was immobilized on the pDA coated nanoparticles *via* Schiff base formation (Fe_3O_4@pDA/HRP), and further employed to functionalize a glassy carbon electrode (GCE) for amperometric H_2O_2 determination.

Materials and methods

Reagents and solutions

HRP (type VI, EC 1.11.1.7, 269 U mg^{-1} solid), DA, hydroquinone, H_2O_2 and all the rest of the chemicals were obtained from Sigma. Electrochemical experiments were performed in 10 mM sodium phosphate, 2.7 mM KCl, 137 mM NaCl, and pH 7.4 buffer solution (PBS). DA solution was prepared in PBS solution (pH 8.5) before use.

Instruments

Glassy carbon electrodes (GCEs, 3 mm diameter) were purchased from CH Instruments Inc., USA. Electrochemical measurements were performed with a DRP-STAT200 potentiostat and data were acquired with Dropview software (DropSens). For all electrochemical measurements, an Ag/AgCl (3 M KCl) and a Pt wire were used as reference and counter electrodes, respectively. Field emission scanning electron micrographs (FE-SEMs) and energy dispersive X-ray spectra (EDS) were obtained using a JEOL JSM-6300 microscope. High-resolution transmission electron microscopy (HRTEM) was performed with a JEOL JEM-3000 F microscope. Transmittance spectra (UV-Vis) of nanoparticles, pDA, HRP solutions and enzymatic studies were recorded in the range of 200–1000 nm with respect to water using a Transpec®photodiode array spectrophotometer. FT-IR spectra were recorded with respect to air, using a Varian 670-IR spectrophotometer in the range of 4000–400 cm^{-1}. The X-ray diffraction (XRD) pattern was recorded using a Philips Panalytical X'Pert powder diffractometer with Cu K_α ($\lambda = 1.540$ Å) radiation. Thermogravimetric analyses were performed with a Perkin Elmer Pyris Diamond TG/DTA apparatus.

Preparation of Fe_3O_4@pDA/HRP nanoparticles

Fe_3O_4 nanoparticles were prepared by the chemical coprecipitation method under a N_2 atmosphere.[30,37,38] $FeCl_3$ (3.24 g) and $FeSO_4 \cdot 7H_2O$ (2.78 g) were dissolved in 200 mL of 1.2 mM HCl solution by ultrasound treatment. Then 1.25 M aqueous NaOH solution (300 mL) was added dropwise under vigorous stirring for 30 min, forming a black Fe_3O_4 precipitate. After vigorous stirring for another 30 min, the precipitate was magnetically decanted and washed thoroughly with ultrapure water till the supernatant solution reached neutrality (pH $\sim$ 7). The resulting black powder was dried in an oven at 40 °C overnight.

For coating with pDA, 500 mg of Fe_3O_4 were dispersed under continuous stirring in 25 mL of 10 mM DA solution (PBS, pH 8.5) for 3 h. After that, polydopamine-modified nanoparticles (Fe_3O_4@pDA) were magnetically decanted, washed thoroughly with ultrapure water to remove the non-reacted DA, and further dispersed in 25 mL of water. To immobilize the enzyme, 50 mg of Fe_3O_4@pDA were dispersed in 1 mg mL^{-1} HRP solution (2.5 mL PBS, pH 7.4) for 3 h under agitation at room temperature. The HRP-modified nanoparticles (Fe_3O_4@pDA/HRP) were magnetically decanted and washed thoroughly with PBS to remove the non-reacted HRP, and further re-dispersed in PBS at 50 mg mL^{-1} final concentration. The enzyme-modified nanoparticles were kept at 4 °C until use.

Preparation of the enzyme electrode

GCEs were first polished with 0.05 μm alumina slurry, rinsed thoroughly with water, then sonicated in water and acetone and finally dried with N_2. GCEs were modified with different volumes of Fe_3O_4@pDA/HRP solution. Finally, biosensors were cured for 1 h at 37 °C.

Electrochemical measurements

A conventional three-electrode system was used for cyclic voltammetry (CV), chronoamperometry (CA) and constant potential amperometry (CPA) analyses with the biosensor as the working electrode, a platinum wire as an auxiliary electrode, and an Ag/AgCl (3 M KCl) electrode as a reference electrode. CV and CPA studies were done in 15 mL PBS containing hydroquinone (HQ) as an electron mediator under constant magnetic stirring.

Enzymatic activity measurements

The free and immobilized HRP-activity was measured by the reaction with H_2O_2 using TMB as a chromogenic substrate. The activity was measured at 25 °C by monitoring the absorbance change at 650 nm with time. 5 μL of 10 mg mL^{-1} Fe_3O_4@pDA/HRP nanoparticles were dispersed in 2.5 mL of PBS and 25 μL of the chromogenic solution (0.1% TMB, 1% H_2O_2) were added and the absorbance was recorded each 30 s. The free HRP-activity was checked using the same protocol but adding 0.9 μg HRP in PBS, the equivalent amount of HRP as that used in the former experiment.

Results and discussion

Preparation of HRP-modified core–shell Fe_3O_4@pDA nanoparticles

The strategy employed to prepare the functionalized magnetic nanoparticles and the HRP-based biosensor is illustrated in Scheme 1. Fe_3O_4 nanoparticles were first synthesized by coprecipitation of Fe^{2+}/Fe^{3+} ions in alkali media,[30,37,38] yielding quasi-spherical and low disperse nanoparticles with an average size of 11 ± 3 nm. These nanomaterials were further coated with an organic thin film through the spontaneous oxygen-mediated self-polymerization of DA in an aqueous solution of pH 8.5, and representative HRTEM images are shown in Fig. 1.

The interplanar distance, measured from the adjacent lattice fringes of the nanoparticles, was about 0.480 nm corresponding to (111) planes of the Fe_3O_4 single crystal with a cubic spinel structure. HRTEM analysis also revealed that the magnetic nanoparticles were coated with a polymeric material with an average thickness of 1.8 ± 0.2 nm. This fact suggests that the nanoparticles were homogenously coated with a thin pDA film, resulting in a low disperse core–shell Fe_3O_4@pDA nanomaterial.

Fig. 2 shows the XRD patterns of Fe_3O_4 and Fe_3O_4@pDA nanoparticles. Fe_3O_4 nanoparticles showed diffraction peaks at 21.09°, 29.98°, 35.39°, 36.41°, 42.95°, 53.23°, 57.03° and 62.60°, corresponding to the (111), (220), (222), (311), (400), (422), (551) and (440) Bragg reflections with interplanar distances of 4.22, 2.98, 2.54, 2.47, 2.47, 2.11, 1.72, 1.61, 1.48 Å respectively. These patterns confirmed the polycrystalline nature of Fe_3O_4 with a cubic spinel structure.[39] The presence of very broad peaks indicated the ultra-fine nature and small crystallite size of the nanoparticles. Thus, the crystallite size was calculated using the Debye–Scherrer equation using the full-width at half diffraction (FWHM) value of the (331) X-ray diffraction line and presented a value of 10 nm, which agrees with HRTEM analysis.

A similar XRD pattern was observed for the core–shell Fe_3O_4@pDA nanoparticles, suggesting that the crystalline structure of the nanomaterial was not affected by coating with the polymer thin film.

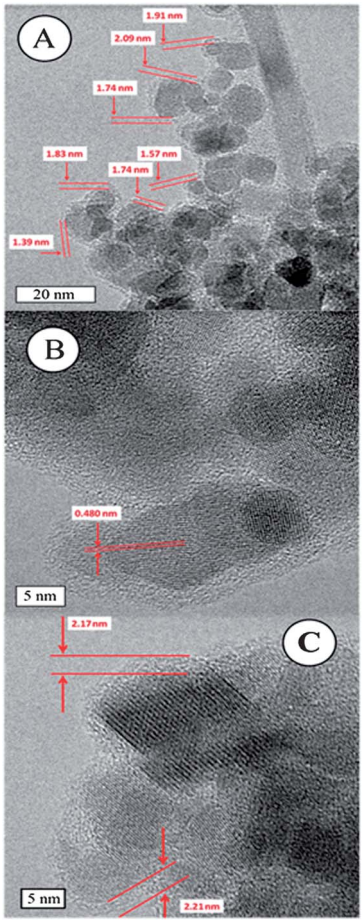

Fig. 1 HRTEM images of Fe_3O_4@pDA nanoparticles at low (A) and high (B) magnifications. The HRTEM image of Fe_3O_4@pDA/HRP nanoparticles at high (C) magnification.

Morphological analysis of the polymer-coated nanoparticles was performed by FE-SEM, and representative images are shown in Fig. 3. As observed, Fe_3O_4@pDA nanoparticles were aggregated in a cluster-like structure, which may be the result of large accumulation of negative charges on the surface and the

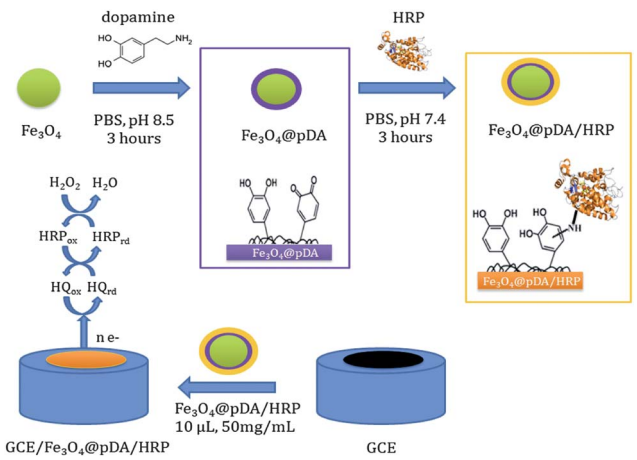

Scheme 1 Schematic illustration of the synthesis of core–shell Fe_3O_4@pDA/HRP nanoparticles and the construction of the Fe_3O_4@pDA/HRP-modified GC electrode.

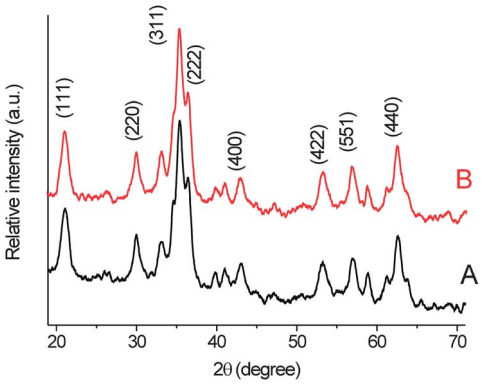

Fig. 2 XRD analysis of Fe_3O_4 (A) and Fe_3O_4@pDA (B) nanoparticles.

adsorption of Fe_3O_4@pDA nanoparticles from the surroundings to achieve inter-molecular force equilibrium. As expected, EDS microanalysis revealed the presence of Fe and O atoms in the nanoparticle structure.

Thermal analysis was performed to confirm and estimate the relative composition of Fe_3O_4 and Fe_3O_4@pDA nanoparticles, and the results are shown in Fig. SM1 (see ESI† for additional details). The weight loss of unmodified Fe_3O_4 at 200 °C was estimated to be 3% of the initial weight, and could be ascribed to the removal of physically adsorbed water. Meanwhile the decrease in the mass of Fe_3O_4@pDA nanoparticles in the same range of temperature was close to 5%, with this change being associated with the weight loss of adsorbed water and DA monomers. The next range of temperature, between 200 and 400 °C, presented a weight loss of 5% for Fe_3O_4 and corresponded to bonded water, but Fe_3O_4@pDA nanoparticles presented a weight loss of about 14% with a broad exothermic peak at 300 °C. This transformation could be ascribed to the thermal decomposition of the chemically attached pDA film from the surface of the Fe_3O_4 nanoparticles, confirming the successful polymer coverage formed on the nanoparticles. Finally, the weight loss of about 1% (both nanoparticles) above 500 °C could be associated with the phase transformation of Fe_3O_4 to Fe_2O_3.

HRP was further immobilized on the core–shell Fe_3O_4@pDA nanoparticles by dispersing the nanosized solid supports in a stirred solution of 1 mg mL^{-1} HRP for 3 h. The presence of free quinone groups on the surface of the pDA-coated nanoparticles favored the covalent immobilization of the enzyme through the formation of stable Schiff base linkages. The amount of immobilized enzyme was estimated to be ~18 μg mg^{-1} support.

This immobilization step was studied by UV-Vis and FT-IR spectroscopy. In this sense, UV-Vis analyses were done for each component (Fe_3O_4, pDA and HRP) and for the final modified nanoparticles (Fe_3O_4@pDA/HRP), and the results are shown in Fig. 4A. The enzyme solution presented a characteristic absorption band at around 420 nm,[21] meanwhile the pDA solution showed a typical absorption band around 350 nm, which results from the formation of the quinone intermediate and the polymerized film.[40] The surface modification of the Fe_3O_4 nanoparticles with these adducts can be confirmed by comparing the spectra of the raw and modified nanoparticle solutions. UV-Vis analysis of Fe_3O_4@pDA/HRP samples revealed that two peaks at 350 nm and 420 nm were superimposed on the characteristic broad absorption peak of Fe_3O_4 nanoparticles, suggesting that the nanoparticles were successfully covered with the pDA film and further modified with the HRP enzyme.

Fig. 4B shows the FT-IR analysis of the Fe_3O_4-based nanomaterials. FT-IR spectra of all Fe_3O_4-based nanomaterials showed a main absorption band around 580 cm^{-1} assigned to the Fe–O stretching modes of the magnetite. pDA-coated nanoparticles showed additional bands in the range of 1000–1700 cm^{-1} which may be ascribed to the aromatic rings of pDA (1614 cm^{-1}), and the amide I, amide II and C–N stretching bands (1639, 1535, and 1230 cm^{-1}, respectively).[29,40] The spectra of HRP-modified nanoparticles were characterized by a broad absorption band around 1200 cm^{-1}, which could be ascribed to the C–N stretching in the new Schiff bases formed during the immobilization step. It should be highlighted that Fe_3O_4 nanoparticles retained their magnetic properties after coating with pDA and further functionalization with HRP, as illustrated in Fig. SM2.†

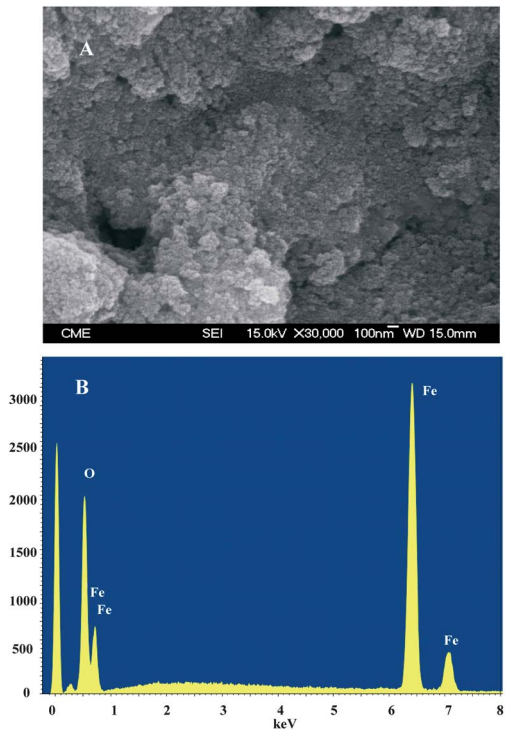

Fig. 3 FE-SEM image (A) and EDS analysis (B) of Fe_3O_4@pDA nanoparticles.

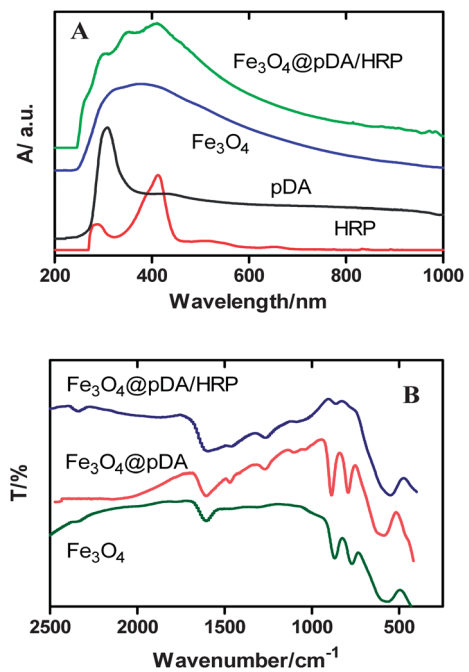

Fig. 4 (A) UV-Vis absorption spectra of free HRP, pDA, Fe_3O_4 and Fe_3O_4@pDA/HRP nanoparticle solutions. (B) FT-IR transmittance spectra of Fe_3O_4, Fe_3O_4@pDA and Fe_3O_4@pDA/HRP nanoparticles.

HRP-modified nanoparticles were characterized by HRTEM. Fe_3O_4@pDA/HRP nanoparticles (Fig. 1C) presented a similar size and distribution to those mentioned above. The film thickness showed a slight increase after HRP-immobilization but the amorphous nature of the pDA film hindered the observation of evident changes in the HRP-modified nanoparticles.

On the other hand, the specific activity of the enzyme was slightly reduced (from 20.8 ± 1.4 U μg^{-1} to 18.5 ± 1.1) after covalent immobilization on the core–shell Fe_3O_4@pDA nanoparticles. Therefore, it can be concluded that the tridimensional enzyme conformation is not significantly altered by the immobilization hence retaining its catalytic activity.

Preparation of the Fe_3O_4@pDA/HRP based biosensor

The potential analytical use of the magnetic core–shell Fe_3O_4@pDA/HRP nanoparticles was evaluated by constructing an electrochemical enzyme biosensor for H_2O_2. For this purpose, GCEs were functionalized with HRP-modified nanoparticles and hydroquinone (HQ) was used as an electrochemical mediator due to its ability to act as an electron shuttle from the redox center of the HRP molecules to the GCE surface, according to the following mechanism:[41]

$$\mathrm{HRP} + \mathrm{H_2O_2} \rightarrow \mathrm{HRP\text{-}I} + \mathrm{H_2O} \quad (1)$$

$$\mathrm{HRP\text{-}I} + \mathrm{HQ_{red}} \rightarrow \mathrm{HRP\text{-}II} + \mathrm{HQ_{ox}} \quad (2)$$

$$\mathrm{HRP\text{-}II} + \mathrm{HQ_{red}} \rightarrow \mathrm{HRP} + \mathrm{HQ_{ox}} \quad (3)$$

$$\mathrm{HQ_{ox}} + 2e^- \rightarrow \mathrm{HQ_{red}} \quad (4)$$

$$\text{Net reaction: } \mathrm{H_2O_2} + 2e^- + 2H^+ \rightarrow 2\mathrm{H_2O} \quad (5)$$

where HRP, HRP-I and HRP-II represent the enzyme peroxidase in the native form and in its two oxidized forms, respectively; and HQ_{red} and HQ_{ox} represent HQ in its reduced and oxidized forms, respectively.

Fig. 5A shows the CVs recorded for the working electrode (GCE/Fe_3O_4@pDA/HRP) in PBS solution, pH 7.4, and containing 1 mM HQ at different scan rates. Both the anodic and the cathodic current peaks (I_{ox} and I_{rd}) increased linearly when the square-root of the scan rate increased (see Fig. 5B) which is characteristic of a diffusion-controlled process.

Fig. 5C shows the CVs of the GCE/Fe_3O_4@pDA/HRP based biosensor in PBS (pH 7.4) in the absence and the presence of HQ at different concentrations. Only a single pair of reversible oxidation/reduction peaks is observed, and peak currents increased with the increase of HQ concentration. This represented the typical electrochemical behavior of HQ.[41] In addition, a noticeable increase of the reduction current and a concomitant decrease of the oxidation current were observed after addition of H_2O_2, Fig. 5D, in agreement with the electrocatalytic mechanism described above. Analogous experiments to those shown in Fig. 5D were done for GCE/Fe_3O_4@pDA configuration. No significant change in the voltammetric responses was observed after H_2O_2 addition (Fig. SM3†)

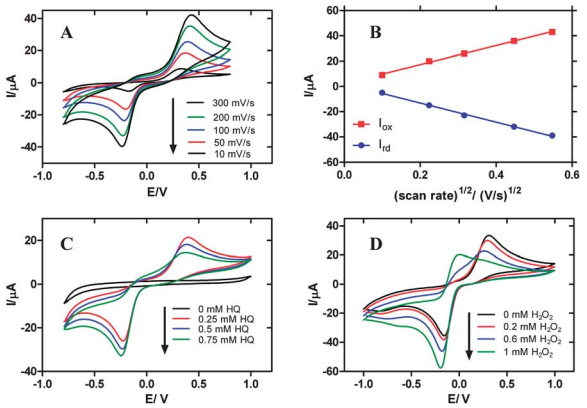

Fig. 5 (A) CVs of GCE/Fe_3O_4@pDA/HRP recorded at 10, 50, 100, 200 and 300 mV s^{-1} in PBS solution, pH 7.4 containing 1 mM HQ. (B) Linear dependence of anodic and cathodic peak currents (I_{ox} and I_{rd}) *vs.* the square-root of the scan rate. (C) CVs for GCE/Fe_3O_4@pDA/HRP recorded in PBS solution, pH 7.4 containing 0, 0.25, 0.5, 0.75 mM HQ (scan rate: 100 mV s^{-1}). (D) CVs of GCE/Fe_3O_4@pDA/HRP recorded in PBS solution, pH 7.4, containing 1.5 mM HQ and 0, 0.2, 0.6, 1 mM H_2O_2 (scan rate: 100 mV s^{-1}).

indicating that, as expected, the presence of HRP prompted the catalytic response to H_2O_2.

The amount of loaded nanoparticles during the preparation of the enzyme electrode was optimized in order to achieve the maximum sensitivity for the amperometric biosensor.

The effect of the modified-magnetic bead amount immobilized on the top of the electrode surface on the amperometric signal is shown in Fig. SM4A.† As can be seen, an increase in the amperometric signal was observed up to 50 μg, the signal decreasing for higher loadings, which was probably due to an increase in the electron transfer resistance for large modified-magnetic bead loadings. In addition, the most favourable working conditions for the enzyme biosensor were optimized. The effect of the applied potential on the amperometric response of the enzyme electrode was evaluated in the range of −250 mV to 100 mV (Fig. SM4B†). The electrode showed a practically constant and higher current value from −250 mV to −150 mV, then the cathodic current decreased steadily with increasing the applied potential. In view of these results, −150 mV was selected as the optimum value for the applied potential. The effect of pH on the amperometric response of the electrode was also checked in the 5.0–9.0 pH range (Fig. SM4C†). The biosensor current exhibited an almost bell-shaped behavior with the highest response at pH 7.4. Finally, the optimum concentration of the electrochemical mediator was also determined. As illustrated in Fig. SM4D,† the cathodic current increased with the concentration of HQ reaching a plateau at 1.2 mM, and this HQ concentration was selected for further studies.

Finally, the biosensor response against temperature was studied in the range of 15 °C to 55 °C (Fig. SM5A†). The amperometric response gradually increased with the temperature, reaching a maximum value at 55 °C. It was further confirmed that the cathodic response of the electrode to temperature in the range of 15–55 °C followed an Arrhenius-

type behavior, as shown in Fig. SM5B.† Accordingly, the activation energy for this enzymatic reaction was estimated to be 55.53 kJ mol^{-1}. Higher working temperatures led to a significant decrease in the electrocatalytic response of the biosensor, which should be attributed to the denaturation/inactivation of the enzyme at these higher temperatures.

Chronoamperometry was used to obtain more information about the electrocatalytic behavior of the developed enzymatic biosensor. Fig. SM6A† shows the current–time plots for the GCE/Fe_3O_4@pDA/HRP configuration recorded following stepping the applied potential from open circuit conditions to −0.15 V in the absence and presence of H_2O_2 in the concentration range of 0.0–1.0 mM. The time evolution of the semi-infinite linear diffusion-controlled current is described by the Cottrell equation:[42]

$$I = nFAC(D/\pi t)^{1/2} \quad (6)$$

where n is the number of electrons consumed ($n = 2$), F is the Faraday constant, A is the electrochemical surface area (0.07 cm^2), C is the concentration (mol cm^{-3}) of the electroactive molecule and D is the diffusion coefficient (cm^2 s^{-1}). The plot of I *vs.* $t^{-1/2}$ at each concentration of H_2O_2 was linear (Fig. SM6B†), and the slopes (m_i) of the resulting straight lines were plotted *vs.* H_2O_2 concentration. The slope of the resulting straight line was then used to estimate the diffusion coefficient of H_2O_2 (Fig. SM6C†), presenting a value of 2.3×10^{-6} cm^2 s^{-1} fairly consistent with data reported elsewhere.[42]

Chronoamperometry was also used for the evaluation of the catalytic rate constant, k_{cat}. At intermediate times, when the current is dominated by the rate of the electrocatalyzed reduction of H_2O_2, the catalytic current (I_{cat}) can be written as follows:[42]

$$I_{cat} = I_L(k_{cat}\pi Ct)^{1/2} \quad (7)$$

where I_L is the current of the biosensor in the absence of H_2O_2 and I_{cat} is the catalytic current due to different H_2O_2 concentrations. Over a limited time frame, the values of I_{cat}/I_L were linearly dependent on $t^{1/2}$, and from its slope k_{cat} was calculated. Finally k_{cat} presents a value of 1.7×10^4 M^{-1} s^{-1} which is in good agreement with data reported in the literature.[43]

In order to demonstrate the benefit of the present configuration, we compared our optimized configuration (GCE/Fe_3O_4@pDA/HRP) with a basic biosensor configuration, where 10 μL of HRP (1 mg mL^{-1}) were adsorbed directly onto the GCE surface (GCE/HRP). Fig. 6 shows the calibration curves of these two configurations. GCE/Fe_3O_4@pDA/HRP showed a sensitivity of 442.14 mA M^{-1} cm^{-2}, a limit of detection, LOD ($S/N = 3$), of 182 nM and an excellent linear range from 0.6 to 800 μM (R^2: 0.999) and acceptable response time ($t_{90\%} = 10$ s). Meanwhile the basic configuration (GCE/HRP) showed a lower sensitivity (100.25 mA M^{-1} cm^{-2}) and linearity (R^2: 0.972) in the same range of concentration with a higher LOD (798 nM). These differences of sensitivities may be justified by taking into account the divergence in enzymatic loading in the two configurations expressed as I_{max} (calibration plateau or maximum current measured under saturated substrate

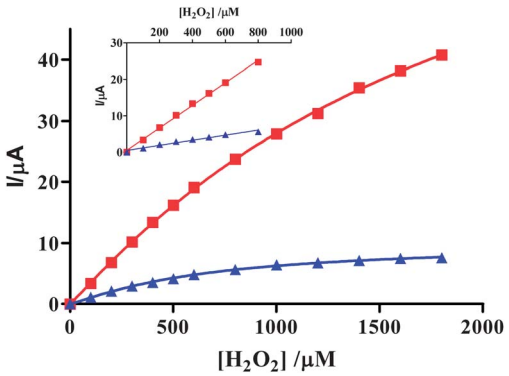

Fig. 6 Calibration curves and linear fitting (inset) obtained using GCE/HRP (triangles) and GCE/Fe_3O_4@pDA/HRP (squares) configurations in PBS (pH 7.4) containing 1.5 mM HQ (CPA, applied potential: −0.15 V).

conditions) ~10.11 and 88.23 μA for GCE/HRP and GCE/Fe_3O_4@pDA/HRP, respectively. Finally, thanks to the synergism between the higher surface (nanoparticles) and higher enzymatic retention (pDA), the present configuration showed better sensitivity[21,41] and LOD[44–47] than previous publications reported in the literature.

In order to study the enzyme kinetics as well as to evaluate the affinity of the immobilized HRP towards H_2O_2 the apparent Michaelis–Menten (Km_{app}) constant was calculated from the electrochemical version of the Lineweaver–Burk equation:[41]

$$1/I_{ss} = 1/I_{max} + Km_{app}/I_{max}C \quad (8)$$

where I_{ss} is the steady state current after the addition of the substrate, C is the bulk concentration of the substrate, and I_{max} is the maximum current. The Km_{app} value of the GCE/Fe_3O_4@pDA/HRP biosensor was determined by the steady state amperometric response curve, which is equal to 3.05 mM, smaller than the values reported previously by other authors using the HRP–ZrO_2 thin film on an Au electrode (8.01 mM),[46] HRP immobilized in the sol–gel-derived ceramic–carbon nanotube nanocomposite film (23.85 mM)[44] and the Fe_3O_4/chitosan modified GCE (21.4 mM).[45] This Km_{app} value, even smaller than that obtained for the free enzyme (Km_{app} = 11 mM),[48,49] confirmed that the immobilized HRP possesses high catalytic efficiency for the reduction of H_2O_2.

The stability of Fe_3O_4@pDA/HRP nanoparticles over time was studied by storing them in PBS (pH 7.4) at 4 °C for a time period of 28 days. Over this time, the response of the modified electrode to 800 μM H_2O_2 was evaluated. As can be seen in Fig. 7, no significant loss of the amperometric response was observed for at least 28 days thus confirming that both the polydopamine film and the immobilized-HRP were stable on the nanoparticle surface as it was suggested previously.[30,34,36]

The selectivity of the GCE/Fe_3O_4@pDA/HRP biosensor was checked under the experimental conditions specified above. The potential interferents tested were glucose, lactate, L-glutamate, choline, uric acid and ascorbic acid. The degree of interference was evaluated by comparing the amperometric responses obtained for 1 mM H_2O_2 in the absence or in the

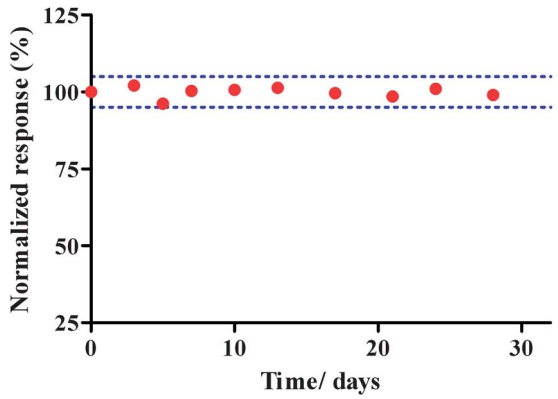

Fig. 7 Control chart constructed to check the stability of Fe_3O_4@pDA/HRP nanoparticles stored in PBS (pH 7.4) at 4 °C. The measurements correspond to the mean value of three measurements for 800 μM H_2O_2. The upper and lower control limits (dashed lines) were set at ±3 SD of the initial value.

presence of each interferent at 0.1 mM concentration. The results listed in Table SM1† demonstrate that no interference was found from glucose, lactate, L-glutamate and choline. However, both uric and ascorbic acids may reduce the HQ produced in the HRP catalyzed reaction and thus interfere with the determination of H_2O_2.

The reproducibility of the amperometric responses obtained with different biosensors constructed following the same protocol was tested for 0.6 mM H_2O_2. The results for five different biosensors yielded a RSD value of 3.9%, thus proving that their fabrication procedure (including both the preparation of Fe_3O_4@pDA/HRP and their magnetic capture on the GCE) was reliable.

Conclusions

In the present work we have developed and characterized a novel functionalized core–shell magnetic nanoparticle (Fe_3O_4@pDA). The present approach is an easy method to modify nanoparticles. The reactive quinones at the surface of the Fe_3O_4@pDA offer a great opportunity to anchor biologically active macromolecules such as antibodies and enzymes. In this way, HRP was used as a proof-of-concept for further modifications (Fe_3O_4@pDA/HRP). Finally, the newly prepared enzymatic nanoconjugates were employed to construct a second-generation biosensor (GCE/Fe_3O_4@pDA/HRP) for H_2O_2 sensing. Experimental variables were optimized in order to improve the biosensor response. All the results discussed above demonstrated that the new H_2O_2 biosensor based on the use of Fe_3O_4@pDA/HRP compares advantageously (in terms of sensitivity, reproducibility and simplicity of the fabrication process) with other biosensor designs.

Acknowledgements

This work has been supported by the programmes INNCORPORA and FEDER (INC-TU-2011-1621), Ministerio de Industria, Turismo y Comercio (TSI-020100-2011-189 and TSI-020100-2010-346), Ministerio de Ciencia e Investigación (TIN2011-28146; CTQ2011-24355), Ministerio de Economía y Competitividad (Research Project CTQ2012-34238) and Comunidad de Madrid S2009/PPQ-1642 programme AVANSENS. R. Villalonga acknowledges Ramón & Cajal contract from the Spanish Ministry of Science and Innovation. We thank Dr Pablo Lorenzo Luis (Inorganic Department of ULL) for helping in UV-Vis measurements.

References

1 S. C. N. Tang and I. M. C. Lo, *Water Res.*, 2013, **47**, 2613–2632.
2 D. Alcantara and L. Josephson, in *Nanobiotechnology Inorganic Nanoparticles vs Organic Nanoparticles*, ed. J. M. de la Fuente and V. Grazzu, Elsevier, 2012, vol. 4, pp. 269–289.
3 P. Tartaj, M. P. Morales, T. González-Carreño, S. Veintemillas-Verdaguer and C. J. Serna, *J. Magn. Magn. Mater.*, 2005, **290–291**, 28–34.
4 S. Singh, K. C. Barick and D. Bahadur, *J. Hazard. Mater.*, 2011, **192**, 1539–1547.
5 J. Chomoucka, J. Drbohlavova, D. Huska, V. Adam, R. Kizek and J. Hubalek, *Pharmacol. Res.*, 2010, **62**, 144–149.
6 S. Laurent, S. Dutz, U. O. Häfeli and M. Mahmoudi, *Adv. Colloid Interface Sci.*, 2011, **166**, 8–23.
7 M. Mahmoudi, S. Sant, B. Wang, S. Laurent and T. Sen, *Adv. Drug Delivery Rev.*, 2011, **63**, 24–46.
8 O. Veiseh, J. W. Gunn and M. Zhang, *Adv. Drug Delivery Rev.*, 2010, **62**, 284–304.
9 C. Sun, J. S. H. Lee and M. Zhang, *Adv. Drug Delivery Rev.*, 2008, **60**, 1252–1265.
10 J. R. McCarthy and R. Weissleder, *Adv. Drug Delivery Rev.*, 2008, **60**, 1241–1251.
11 J. Huang, B. Han, W. Yue and H. Yan, *J. Mater. Chem.*, 2007, **17**, 3812–3818.
12 J. Huang, X. Li, Y. Zheng, Y. Zhang, R. Zhao, X. Gao and H. Yan, *Macromol. Biosci.*, 2008, **8**, 508–515.
13 G. Bayramoğlu, M. Yılmaz, A. Ü. Şenel and M. Y. Arıca, *Biochem. Eng. J.*, 2008, **40**, 262–274.
14 J. Wang, D. Song, H. Zhang, J. Zhang, Y. Jin, H. Zhang, H. Zhou and Y. Sun, *Colloids Surf., B*, 2013, **102**, 165–170.
15 E. Katz, I. Willner and J. Wang, *Electroanalysis*, 2004, **16**, 19–44.
16 N. Jaffrezic-Renault, C. Martelet, Y. Chevolot and J.-P. Cloarec, *Sensors*, 2007, **7**, 589–614.
17 R. Rawal, S. Chawla and C. S. Pundir, *Biosens. Bioelectron.*, 2012, **31**, 144–150.
18 X. Chen, J. Zhu, Z. Chen, C. Xu, Y. Wang and C. Yao, *Sens. Actuators, B*, 2011, **159**, 220–228.
19 S. Wang, Y. Tan, D. Zhao and G. Liu, *Biosens. Bioelectron.*, 2008, **23**, 1781–1787.
20 H. Teymourian, A. Salimi and R. Hallaj, *Biosens. Bioelectron.*, 2012, **33**, 60–68.
21 Y.-H. Won, D. Aboagye, H. S. Jang, A. Jitianu and L. A. Stanciu, *J. Mater. Chem.*, 2010, **20**, 5030–5034.
22 A. Sassolas, L. J. Blum and B. D. Leca-Bouvier, *Biotechnol. Adv.*, 2012, **30**, 489–511.

23 G. Remington, in *Serotonin–Dopamine Interaction: Experimental Evidence and Therapeutic Relevance*, ed. G. Di Giovanni, V. Di Matteo and E. Esposito, Elsevier, 2008, vol. 172, pp. 117–140.
24 M. J. Hurley and P. Jenner, *Pharmacol. Ther.*, 2006, **111**, 715–728.
25 J. L. Katz, A. H. Newman and S. Izenwasser, *Pharmacol., Biochem. Behav.*, 1997, **57**, 505–512.
26 H. Lee, S. M. Dellatore, W. M. Miller and P. B. Messersmith, *Science*, 2007, **318**, 426–430.
27 H. Lee, J. Rho and P. B. Messersmith, *Adv. Mater.*, 2009, **21**, 431–434.
28 R. Luo, L. Tang, J. Wang, Y. Zhao, Q. Tu, Y. Weng, R. Shen and N. Huang, *Colloids Surf., B*, 2013, **106**, 66–73.
29 L.-P. Zhu, J.-H. Jiang, B.-K. Zhu and Y.-Y. Xu, *Colloids Surf., B*, 2011, **86**, 111–118.
30 Y. Li, C. Qin, C. Chen, Y. Fu, M. Ma and Q. Xie, *Sens. Actuators, B*, 2012, **168**, 46–53.
31 H. O. Ham, Z. Liu, K. H. A. Lau, H. Lee and P. B. Messersmith, *Angew. Chem., Int. Ed.*, 2011, **50**, 732–736.
32 K. Yang, J. S. Lee, J. Kim, Y. B. Lee, H. Shin, S. H. Um, J. B. Kim, K. I. Park, H. Lee and S.-W. Cho, *Biomaterials*, 2012, **33**, 6952–6964.
33 S. M. Kang, N. S. Hwang, J. Yeom, S. Y. Park, P. B. Messersmith, I. S. Choi, R. Langer, D. G. Anderson and H. Lee, *Adv. Funct. Mater.*, 2012, **22**, 2949–2955.
34 J. Ryu, S. H. Ku, H. Lee and C. B. Park, *Adv. Funct. Mater.*, 2010, **20**, 2132–2139.
35 C. Xu, K. Xu, H. Gu, R. Zheng, H. Liu, X. Zhang, Z. Guo and B. Xu, *J. Am. Chem. Soc.*, 2004, **126**, 9938–9939.
36 H. Peng, X. Zhang, K. Huang and H. Xu, *J. Wuhan Univ. Technol., Mater. Sci. Ed.*, 2008, **23**, 480–485 LA-English.
37 L.-L. Pang, J.-S. Li, J.-H. Jiang, Y. Le, G. L. Shen and R.-Q. Yu, *Sens. Actuators, B*, 2007, **127**, 311–316.
38 C. Zou, Y. Fu, Q. Xie and S. Yao, *Biosens. Bioelectron.*, 2010, **25**, 1277–1282.
39 H. E. Ghandoor, H. M. Zidan, M. M. H. Khalil and M. I. M. Ismail, *Int. J. Electrochem. Sci.*, 2012, **7**, 5734–5745.
40 C. Cheng, S. Li, W. Zhao, Q. Wei, S. Nie, S. Sun and C. Zhao, *J. Membr. Sci.*, 2012, **417-418**, 228–236.
41 X. Wei, T. Liu, J. Li and X. Chen, *Int. J. Electrochem. Sci.*, 2011, **6**, 4953–4966.
42 P. Salazar, M. Martín, R. D. O'Neill, R. Roche and J. L. González-Mora, *J. Electroanal. Chem.*, 2012, **674**, 48–56.
43 A. Karyakin, E. E. Karyakina and L. Gorton, *J. Electroanal. Chem.*, 1998, **456**, 97–104.
44 H. Chen and S. Dong, *Biosens. Bioelectron.*, 2007, **22**, 1811–1815.
45 X. Tan, J. Zhang, S. Tan, D. Zhao, Z. Huang, Y. Mi and Z. Huang, *Electroanalysis*, 2009, **21**, 1514–1520.
46 Z. Tong, R. Yuan, Y. Chai, Y. Xie and S. Chen, *J. Biotechnol.*, 2007, **128**, 567–575.
47 X. Li, J. Wu, N. Gao, G. Shen and R. Yu, *Sens. Actuators, B*, 2006, **117**, 35–42.
48 S. Q. Liu and H. X. Ju, *Anal. Biochem.*, 2002, **307**, 110–116.
49 Y. Xiao, H. X. Ju and H. Y. Chen, *Anal. Chim. Acta*, 1999, **391**, 299–306.

